International Journal of Thermofluids 25 (2025) 101015

Contents lists available at ScienceDirect

International Journal of Thermofluids

journal homepage: www.sciencedirect.com/journal/international-journal-of-thermofluids

Marine energy harvesting from fluid flow via vortex induced vibrations

Zahrapanah Razaviyn [a], Milad Heidari [b], Sivasakthivel Thangavel [b], Vikas Verma [c], Ashwani Kumar [d,f,*], Ashok Kumar Yadav [e]

[a] Faculty of Engineering, Persian Gulf University, Boushehr, Iran
[b] Department of Mechanical Engineering, Global College of Engineering and Technology, Muscat, Oman
[c] Department of Energy, Tezpur University Assam 784028, India
[d] Technical Education Department Uttar Pradesh Kanpur 208024, India
[e] Department of Mechanical Engineering, Raj Kumar Goel Institute of Technology, Ghaziabad 201017, India
[f] Department of Mechanical Engineering, Graphic Era deemed to be University Dehradun, 248002, India

ARTICLE INFO

Keywords:
Vortex induced vibrations
Finite volume method
Energy extraction
Turbulent Flow
Marine Energy

ABSTRACT

This research study highlights into the dynamics of vortex-induced vibrations (VIV) in a rigid cylinder, employing computational fluid dynamics (CFD) simulations validated against experimental data. The primary objective is to explore the potential of harnessing energy from fluid flow-induced vibrations, particularly at lower flow speeds, which are traditionally overlooked by conventional turbine technologies. The CFD simulations investigated the transverse vibrations of a rigid cylinder with elastic support across a wide range of Reynolds numbers. The numerical results were compared with experimental data obtained from the University of Michigan, demonstrating strong correlation, especially for a spring stiffness of 1200 N/m, zero damping, and a relative mass of 1.89. Under these conditions, the maximum relative amplitude of 1.75 was achieved at a Reynolds number of 90,000. The study revealed that increasing spring stiffness up to 1200 N/m enhances the oscillation amplitude. However, further increases in stiffness lead to a decrease in amplitude. Damping and relative mass also significantly influence the vibration behavior. Lower relative masses and damping ratios result in larger amplitude oscillations over a broader range of Reynolds numbers. These findings underscore the feasibility and potential of energy extraction from fluid flows that were previously considered unsuitable. The quantitative insights provided in this study offer valuable guidance for the design and optimization of VIV energy converters. Future research should focus on long-term simulations to further elucidate the impact of these parameters on the performance and durability of such systems.

1. Introduction

Harnessing the dynamic forces within the fluid flow for sustainable energy extraction has spurred innovative research endeavors. By capitalizing on the unique phenomenon of vortex-induced vibrations (VIV), the manuscript ventures into a realm where conventional turbine technologies deem the flow velocities as suboptimal. With an emphasis on computational fluid dynamics (CFD) and comprehensive parameter analyses, this research aims to unravel the intricacies of VIV energy conversion from a rigid cylinder within a specified Reynolds number (Re) range. This innovative approach offers a promising avenue for efficient, clean energy generation in fluid flows previously overlooked by conventional energy extraction methods. The quest for sustainable energy solutions has been an evolving frontier, and this manuscript explores deep into the realms of renewable energy extraction. This study investigates the energy potentials within turbulent fluid flows, contributing to advancements in alternative energy generation methods.

The vibrational motion of objects that are located vertically against the flow of a fluid is the vibration of the stimulus caused by the vortex. The main cause of this phenomenon is the formation of vortices and the separation of flow from the surface of the body. Vibrations caused by vortices are oscillations that an object carries in the flow of water or air. These vibrations create mechanical energy that can be transformed into a power take-off system such as a hydraulic pump or linear generator. Power plants have made rapid progress thanks to its similarity to hydroelectric plants. However environmental problems have brought about major changes to the methods. There are many types of wave environments. Some float on water and some are installed on the beach

* Corresponding author.
E-mail address: drashwanikumardte@gmail.com (A. Kumar).

https://doi.org/10.1016/j.ijft.2024.101015

Available online 11 December 2024

(Falnes, J. (2007). A review of wave-energy extraction. *Marine Structures*, 20(4), 185–201). Also, the way they interact with the waves and thus the type of motion they absorb is very different. Small samples some wave systems have been developed in the world up to now. Generally, the self-stimulating vibrations of bodies are vertically placed against a fluid flow. The cause of this phenomenon is the formation of vortices on the top and bottom of the cylinder and their separation. The existence of a vortex means the formation of a low-pressure region behind the cylinder, which is equivalent to the introduction of a force on the cylinder. These vibrational movements can be very large for elastic bodies, which are subject to uniformity of flow. Bernitsas and Ragavan (2005) [1,2] invented a converter (VIVACE) that would contain the kinetic energy of the ocean and rivers at low speeds of 2 nats. The VIVACE converter includes a rigid cylinder with a spring support, which converts the mechanical energy into another form of energy. Lee et al. [3] examined the effects of damping coefficients and spring hardness coefficients on the performance due to vortexes for smooth cylinders in 2011. The limits of the relative decay rate were reported as 0 to 16 and the range of hardness coefficient of 400 to 1800 Nm/m. Chang [4] examined the effect of surface roughness on this phenomenon. In this study, the effect of surface roughness on increasing the correlation length, fixing the spraying point, causing negative damping, and accelerating the transition phenomenon were investigated. Some studies have investigated the effect of spring, stiffness coefficient, damping coefficient, and cylindrical roughness on the amplitude and frequency of vibration [3–6]. One of the important parameters affecting the power of the VIVACE converter is the maximum oscillation amplitude that has been investigated in the form of vibrations caused by vortices in many studies [7–13].

These studies have been carried out in relative masses and attenuation and the maximum amplitude has been reported. The feature of this converter is its flexibility and scalability. This converter can be exploited by the parameters involved, including cylinder diameter, damping coefficient, hardness coefficient, and Re in the microwatt scale up to megawatt [14]. In 2004, Sarpkaya [15] concluded that vibrations resulting from vortices are inherently self-limiting phenomena, exhibiting fluctuations in the flow field across shear layers on both sides of the body. Notably, the vertical vibrations of the cylinder, perpendicular to the flow and occurring at the frequency of vortex production, significantly impact the vortex production process. A wide range of studies investigated free and forced vibrations caused by vortices both numerically and experimentally (Williamson, C. H. K., & Govardhan, R. (2004). Vortex-induced vibrations. *Annual Review of Fluid Mechanics*, 36, 413–455) (Ran, Li., Jie, Gong., Wei, Chen., Jie, Li., Wei, Chai., Chang-Kyu, Rheem., Xiaobin, Li. (2023) Numerical Investigation of Vortex-Induced Vibrations of a Rotating Cylinder near a Plane Wall. Journal of Marine Science and Engineering, Available from: 10.3390/jmse11061202). One of the important parameters used in the VIVACE converter is the vibrational range of vortices. This parameter has been measured in numerous numerical and experimental studies. Re, surface roughness, damping, spring coefficient, and relative mass have the greatest impact on the range of vibrations caused by vortices. Other important factors in vibrations caused by vortices are frequency and phase angle. The latter is the angle at which the lifting force is superior to the displacement of the object. In the vibrations caused by vortices, the angle of the phase is said to be the angle at which the lifting force is superior to the displacement of the object. In other words, this variable shows the coexistence or non-alignment of the lift with displacement.

Khalak et al. [16] concluded that the angle of the phase in different branches of the response was different. In the upper branch, this angle reaches its minimum. Relative mass is one of the variables that play a vital role in vibrations caused by vortices, which is widely discussed in the research. According to the results of Guardan et al. [17], it can be shown that by decreasing relative mass, the frequency of oscillation during the phenomenon of synchronization will be greater than the natural frequency of the system. Guardan et al. proved the existence of a relative critical mass that is less relative to relative masses than those of a very large range. They also concluded that as the Re increases, the critical range will still be large, and virtually no coincidence behavior will occur for Re. In this study, numerical simulation has been used to evaluate the performance of the Variable Speed Drive (VSD) converter. Zou et al. [18] have investigated a Computational Fluid Dynamics (CFD) tool that is set up to simulate Variable Submerged Body Wave Energy Converter (VSB WECs), using the ANSYS 2-way fluid-structure interaction (FSI) tool. The dynamic behavior of a Variable Submerged Body Wave Energy Converter (VSB) WEC was simulated in this CFD-based Numerical Wave Tank (CNWT), in open sea conditions. They concluded that the tested device undergoes a significant deformation in response to the incoming waves before it reaches a steady-state behavior. Jafari et al. [19] studied the capability of Flow-3D commercial software in the simulation of a specific ocean wave energy converter.

The wave energy converter (device targets wave energy conversion) was simulated inside a wave tank including water. Furthermore, Reynolds Averaged Navier-Stokes equations were coupled with the volume of fluid (VOF) model to generate three-dimensional numerical linear propagating waves as well as solve the fluid flow [20–24]. Their results indicated the capability of Flow-3D software for modeling fluid-structure interaction (FSI) problems including wave motions. In general, numerical methods have advantages in comparison with other methods. It's essential to assess the reliability of a numerical approach to ensure that the results obtained are trustworthy and can be used for making informed decisions. The reliability of numerical and computational methods has been already shown in many studies [25–28]. Given the fact that the number of parameters affecting such a diode is high, using numerical methods makes the researcher able to change the parameters [29–32]. On the other hand, there is no proper examination of such a system. Its specifications are limited and at high speeds, there is a potential for damaging the laboratory transducer. By using numerical methods, we can predict the behavior of the VS converter system in the real environment and use the results of numerical methods to investigate and design the real model. The purpose of this study is to investigate the ability of computational fluid dynamics to simulate the VOA system and examine various parameters on this converter. The data can be used numerically for optimal design. Then, the physical model of the VIVACE converter was examined.

An enhanced collocation method has been suggested in one study to discretize the multi-parameter, fourth-order non-linear Kuramoto-Sivashinsky (K-S) equation [33]. Quantic Hermite splines were used to discretize the spatial direction, while a weighted finite difference scheme was used to discretize the temporal direction. By dividing the equation into coupled equations and adding a new differentiable function, the equation of fourth order was simplified to a second-order form. The convergence was improved by this splitting in the direction of space. Splitting resulted in a twofold increase in computational work, but the process was nonetheless straightforward and productive. Using the Von-Neumann method, the technique's unconditional stability has been established [33]. Another study investigated Vortex-induced vibrations (VIVs) of a flexible cylinder based on a wake oscillator model. The dynamics of the flexible cylinder was described based on the linear Euler–Bernoulli beam theory, and a wake oscillator model was uniformly distributed along the cylinder to model the hydrodynamic force acting on it. The cross-flow VIV primarily occurred in the local cross-flow direction, and a transition of its vibrating direction happened at the interface of the two flows. Energy analysis showed that this transition is boosted by a specific energy transfer pattern between the structure and the flow, which excites the vibration of the cylinder in some directions while damps it in others [34].

The governing equations for fluid dynamics and the rigid body motion equation were presented and the scope of the solution, boundary conditions, and computational grid were studied. The vibrations induced by vortices around a rigid cylinder with elastic support were

analyzed within a Reynolds number (Re) range of 30,000 to 130,000, considering a single degree of freedom. The data obtained from the simulation with the reported values of the experiments performed at the University of Michigan Laboratory has been verified. With variations in the spring stiffness coefficient, relative damping, and relative mass, the cylindrical performance is investigated with different Re. The main results are extracted from the forthcoming research and based on these results, suggestions for future studies are presented [35–37]. Conducting experiments on wave energy converters is the most reliable way to evaluate different functional scenarios, design, and optimization. However, the high cost of building different models and creating different laboratory layouts is an important problem when using the laboratory method. Replacing laboratory methods with theoretical tools is a good solution to reduce the cost of studying different scenarios. In this research, a numerical tool is developed to simulate the behavior of a submerged cylinder due to encountering a slow or turbulent flow within the framework of assumptions and theoretical models. As stated in this study, using CFD, transverse vibrations caused by eddies and flow have been investigated for a rigid cylinder of one degree of freedom with elastic support in a range of Re. For this purpose, the parameters of the spring stiffness coefficient, damping coefficient, and relative mass have been changed in the StarCCM software environment based on the finite volume method [38–39].

Pandey et al. investigated the capability of VIV phenomenon in generating alternative energy from water currents and underlying concepts of the design and operation of the VIVACE converter [40]. A mathematical model was developed, and design scalability for a wide range of applications was presented. To maximize the potential of energy harnessing, the effects of lock-in phenomenon and different geometries of bluff bodies are discussed. It was observed that while renewable technologies like solar and wind energy are in use, they have inherent limitations that can be mitigated by implementing hybrid systems. Different designs of VIV converters are required to be numerically and experimentally researched to trigger the advancement of based converter technology to fulfil ever-increasing global energy demand by renewable energy sources [40]. Fang et al. proposed an auxetic nNar VIV energy harvester. For the first time, the advantages of monostable softening behavior using magnetic attraction were investigated [41]. It is found theoretically and experimentally that the monostable softening can broaden the working wind speed range whereas decreasing the peak energy output. Thus, the auxetic structure is proposed to compensate the decrease of peak energy output with the monostable softening due to its negative Poisson's ratio and high stress distribution [41]. A study examined the validity of a parameter optimization approach to maximize the energy capture efficiency using VIV. The Box–Behnken design response-surface method (RSM-BBD) applied for optimization purpose. The proper combinations of these operating variables were then identified in this regard. Generally, the optimal operating conditions predicted using the response-surface method agreed well with those simulated using our CFD model. The number of experiments was successfully reduced somewhat, and the operating conditions that lead to the highest efficiency of energy harvesting using VIV were determined [42].

To investigate the effective factors in the mechanism of the flowing vortex phenomenon, the flow around the horizontal cylinder exposed to the uniform flow of water, in the state of turbulent flow has been discussed. Therefore, the purpose of this study is to study the ability of computational fluid dynamics in simulating the Vivas converter system and check different parameters on this converter. The data of this numerical method can be used for designing an optimal converter [43–45]. To check the accuracy of the method, the data obtained from the simulation have been compared and verified with the values reported from the experiments conducted in the laboratory of the University of Michigan. With changes in the spring stiffness coefficient, relative damping, and relative mass, the performance of the cylinder was checked at different Reynolds numbers. The simulations are estimated for a rigid cylinder of one degree of freedom with elastic support in the range of Re between 30,000 and 130,000. The maximum amplitude of the cylinder vibrations caused by the flow occurs for a spring with a stiffness coefficient of 1200 N/m and a relative damping of zero and a relative mass of 0.94 at a Re number of 90,000 [39–43]. Also, this study was conducted in the Persian Gulf experimentally, which has not been done in the past due to the prevailing regime of its waves, and due to the existence of many natural and gas energy resources in this area. However, this study has examined the possibility of producing energy from these sources in this region due to the lack of rain and climate changes due to solar and sea energy and the lack of water. A tidal power plant can be built considering the regime of the Persian Gulf [46–48].

The goal of obtaining the maximum amplitude of oscillation according to the amount of power created by the generator directly depends on the speed, amount of displacement, and frequency of the vibrating cylinder. In recent years, researchers investigated some VIV energy harvesting designs and modeling methods [49–50]. Extensive studies on the vibrations caused by vortices have been carried out numerically and experimentally. The investigation on this phenomenon is divided into two separate categories free and forced vibrations. Although the Vivas converter is affected by free vibrations, nevertheless, the study of forced vibrations can be helpful in improving the performance of this converter and understanding the physical phenomena related to this system [51–53]. To maximize electricity generation from vortex-induced vibrations, this study aims to optimize the amplitude and frequency of cylinder oscillations. By leveraging experimental data and computational fluid dynamics (CFD) simulations, this study investigate the hydrodynamic forces and vortex shedding patterns around a horizontally submerged cylinder exposed to a uniform water flow. The CFD simulations, employing the finite volume method, accurately replicate the experimental conditions, including turbulent flow and the resulting vertical forces on the cylinder. By systematically varying key parameters within the CFD model, study aims to identify the optimal conditions for maximizing the amplitude of vibration. The comparison of numerical and experimental results will validate the accuracy of the CFD simulations and provide valuable insights into the underlying physics of vortex-induced vibrations. These insights will be instrumental in designing efficient energy harvesting devices that can effectively extract energy from fluid flow.

2. Methods

As indicated, the computational domain provides a similarity to a stretch pool by creating a control volume around the object to examine the behavior of the object. Choosing the right dimension for the validity of the numerical approach has already been investigated in many studies. The computational domain is one of the important steps in numerical simulation. If the dimensions of the computing range are smaller than the required limit, the simulation will be met by reducing the accuracy of the response. Because in this case the flow of water after collision with the object quickly reaches the boundaries and the reflection of the flow from the boundary will again hit the object. On the other hand, the choice of a large domain will increase significantly the volume and time of computing. The diameter of the cylinder is 0.0889 m and the cylinder length is 0.9144 m. The entire computational domain considered in this article is a rectangular cube with the dimensions shown in Fig. 1. The computational amplitude is assumed to be at the back of the 6-meter cylinder, thus ensuring that the flow is not reflected from this boundary. The position of the cylinder relative to the free surface, as well as the floor of the compass range of 0.5 m, is not constant in this position and the cylinder in the vertical direction will have oscillating motion. Also, the height of computational amplitude above and below the free surface is 0.5 and 1 m, respectively.

According to the shape, the lateral aspect of the computational domain is considered to be a cylinder of 0.1 m. This distance was constant throughout the range and led to the formation of an amplitude of

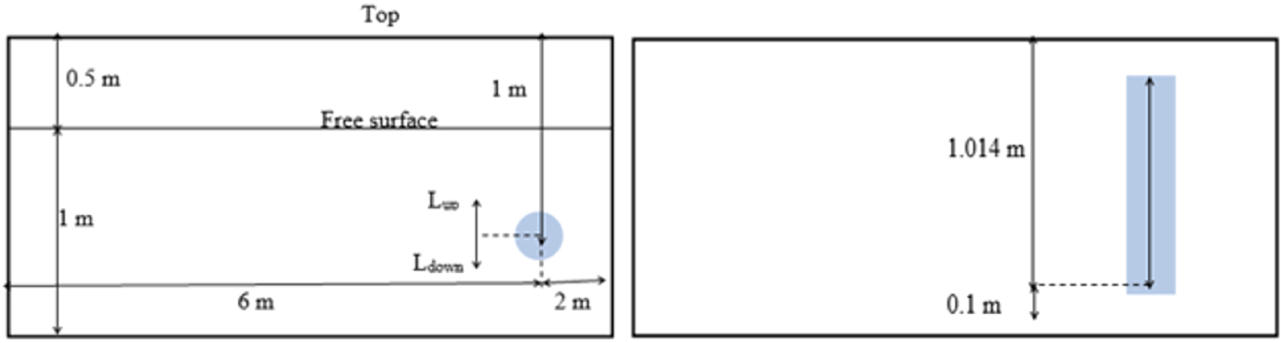

Fig. 1. The shape of the computational domain, face-to-face and top view.

1.04 m. The boundary conditions used in the computational domain are shown in the Table (1). According to Fig. 2, both air and water velocities enter the boundary of input to the computation domain and exit from the opposite direction. In this way, the boundary condition of the input and output of the computing domain is considered as the vertical speed and output pressure, respectively. The conditions of the stretching pond and the freewheel are provided to check the performance of the converter. The boundary condition of the rigid body (wall) is applied to the surface of the object and the upper and lower boundaries of the computational domain. The boundary condition of two side walls in the computational domain is also defined as symmetry in accordance with Table 1.

Simulations are defined in three-dimensional space and, given the model's freedom of movement, the flow is considered unsteady. In unstable physical conditions, it is necessary to define a specific time step. Choosing a small step will help increase simulation accuracy and, on the other hand, increase the amount of computing and time resolution. The time step considered in the simulations performed in this article is 0/0001 s. The fluid in the computational range is defined as the Eulerian phase, which includes air, water, and combinations of these two phases.

The composition characteristics of these two fluids will also be calculated according to the percentages of each one based on the governing equations of the fluid volume method. Also, due to the interaction between the flow of water and the moving cylinder below the water surface, the flow regime is considered to be confusing. The Ca-Epsilon model is also used to solve the equations governing the turbulent flow regime. The morphing model has also been used to allow cylinder movement to move freely in line with Hugh's motion. In general, the governing equations of numerical software are based on Navier Stokes equations. The cylinder will move due to the flow of water at a specified speed to the cylinder under the water surface.

Depending on the degrees of freedom defined for the vortex converter, the cylinder can only fluctuate along the vertical axis. After defining a computational domain around the cylinder and determining the physical conditions governing this domain, it is necessary to process the computing domain networking. In the computational domain grid, fine-volume control volumes are defined on the surface of the object and the computational domain, and the governing equations governing the flow physics are solved at any time in this volume of control. In this study, various types of networks used in StarCcm software have been

Table 1
Boundary conditions of the computational domain.

Domain page	Boundary conditions	Kind of
The object	The wall	Non-slip
Page down	The wall	Non-slip
Top page	The wall	Non-slip
entering page	Stream input speed	Vertical speed
Output page	Stream Output Pressure	Hydrostatic pressure
Side plates	Symmetry	–

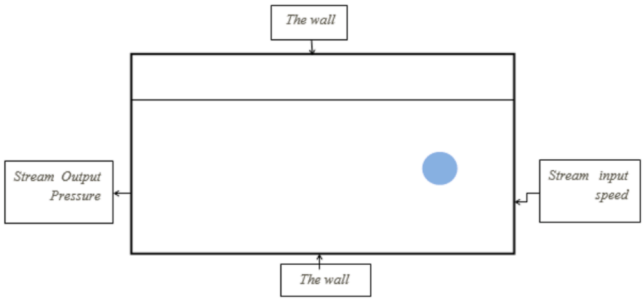

Fig. 2. Boundary conditions in the computational domain.

used. The main network used in this superficial networking simulation has been applied throughout the computational domain, on the surface of the object and boundaries with a growth rate of 1.05. Fig. 3 shows the gridding on the cylinder surface and the computational domain and its growth rate with the distance from the object. The second network used is the luminal prism network around the cylinder. This kind of network will help to improve the flow of contact with the object by creating parallel layers around the cylinder. The laminar primer network is represented in the form of six parallel layers of a thickness of 0.005 m.

In addition to the two types of networks mentioned, a network-based type of terminal is used at the free level. This type of network provides the ability to specify network dimensions in each axis of coordinates. Three control volumes are defined in the computational domain. This way, in each of these three sizes, it is possible to control the mesh size and dimensions. Initially, a free- volume is created in the free surface position. The purpose of this volume is to control the height of free surface cells to check the fluid type in each cell more accurately. Therefore, in this volume control, a vertical mesh is used along the z-axis. Also, for a more accurate analysis of the flow profile around the cylinder and the control of its path, two separate control volumes around the cylinder and its propulsion path are defined, which is used in both cases of the mesh. The convergence of the mesh to obtain the optimal

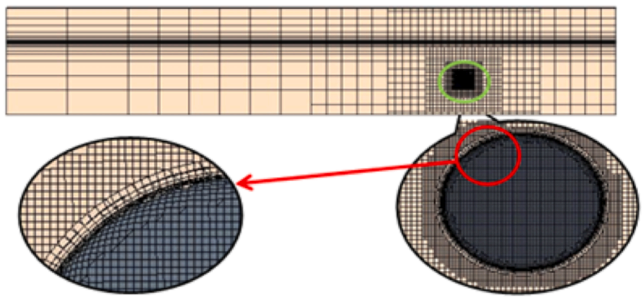

Fig. 3. Computational domain networking.

mesh size for the simulation is investigated.

Fig. 4 shows a schematic of the components of the designed and manufactured VIVACE converter. This device is inspired by the VIVACE converter, as described in the work of Bernitsas and his research group. The converter is made of a plexiglass tube (1) with a diameter of 63 cm, a thickness of 5 mm, and a length of 70 cm. This cylinder is the main cylinder of the device which will be placed in front of the flow and the flow will pass through the outer surface of this cylinder and the cylinder will oscillate according to the applied conditions. To connect the cylinder to the support base, two plexiglass gaps are used at both ends of the tube. These chats seal the two ends of the tube and are connected to the support base using the screw on it to limit the cylinder movements only in the vertical direction and not to allow the cylinder to move in the transverse direction. The performance of the constructed transducer is investigated in the Persian Gulf. A view of the transducer tested in the Persian Gulf is shown in Fig. 4, f. The performance of the device in water has been acceptable for the initial stages of construction. After construction, the converter has been tested in the Persian Gulf. The test of the converter has been done only in the preliminary stage and only the performance of the device has been examined. After installation on the coast of the Persian Gulf, the device has had an oscillating movement due to the speed of the water flow. Investigations to complete this converter will be done shortly and in the next research. The first research is about how to place the motion measurement system.

According to the defined variables, the relationship between amplitude and frequency can be observed. In this part, variables and dimensionless numbers are examined. A smooth cylinder with a diameter of D = 0.0889 cm is used for simulation. The cylinder is simulated in three dimensions and different networks (Table 2 (a-b)). The variables and dimensionless numbers used in this article are shown in Table 2 (b). In this case, variables and non-dimensional numbers are investigated. To simulate a flat cylinder with a diameter of D = 0.889 cm.

The convergence of the mesh to obtain the optimal mesh size for the simulation was investigated. Simulation in Re from 60,000 to 90,000 for K = 1200 N / m, $\zeta = 0$, and $m^* = 1.89$ in numbers 301,223, 474,344, and 646,321 networks. Then the results are compared with the experimental results and the accuracy of the solution is evaluated. Fig. 5 shows the comparison of the results with different cell numbers. Based on Fig. 5, it is clear that by increasing the number of networks used from 301,223 to 474,344, the accuracy of the solution is optimally improved and the error rate is reduced. Also, with a further increase in the number of cells to 646,321, the results will not change significantly. However, as the number of networks increases, the solution time will always increase.

According to Tables 2 & 3, the simulation process lasted 2 days using grid number 2 including 474,344 grid cells. While increasing the number of networks used to 646,321 networks, the resolution time increases to 5 days. By comparing the results of both types of networks, it is clear that the results obtained from Networking 1, despite the low time, are desirable and the error rate can be neglected. In this way, other simulations will be performed using this grid. At this stage, the vibration

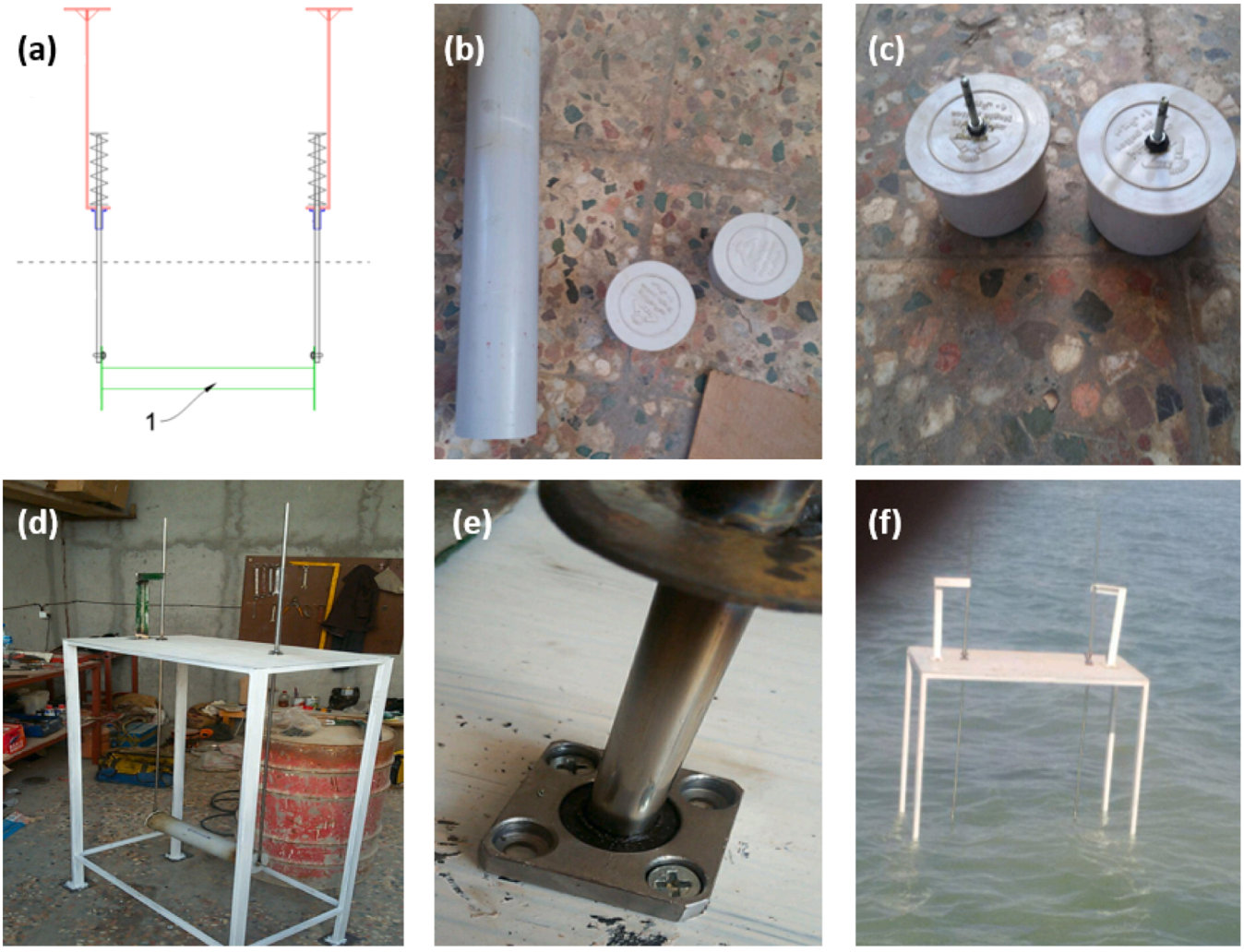

Fig. 4. A systematic arrangement of VIVACE, (a) VIVACE Designed Model, (b, c, e) Pipe and gap arrangement, (d) VIVACE setup, (f) view of the converter inside the Persian Gulf.

Table 2
(a): Time-solving in any number of networks (b): Variables and non-dimensional numbers.

(a)

	Networking 3	Networking 2	Networking 1
Network number	301,223	474,344	646,321
Time step	0001/0	0001/0	0001/0
Solving time (day)	1	2	5

(b)

No number	Relation	Definition
A^*	A/D	Relative domain
m_d	$\frac{\pi}{4}\rho D^2 L$	Transitional mass
m_a	Camd	Added mass
C_a		Extra mass coefficient
m		Cylinder mass
m^*	m/md	Relative mass
ζ	$\frac{c}{2\sqrt{k(m+m_a)}}$	Relative Damping
f_{osc}		Frequency of moving cylinder
$f_{n,\ water}$	$\frac{1}{2\pi}\sqrt{\frac{k}{(m+m_a)}}$	Natural frequency in water
$U_{r,air}$	$\frac{U}{f_{n,air}D}$	Relative velocity based on the natural frequency in the air
$U_{r,water}$	$\frac{U}{f_{n,water}D}$	Relative velocity based on natural frequency in water

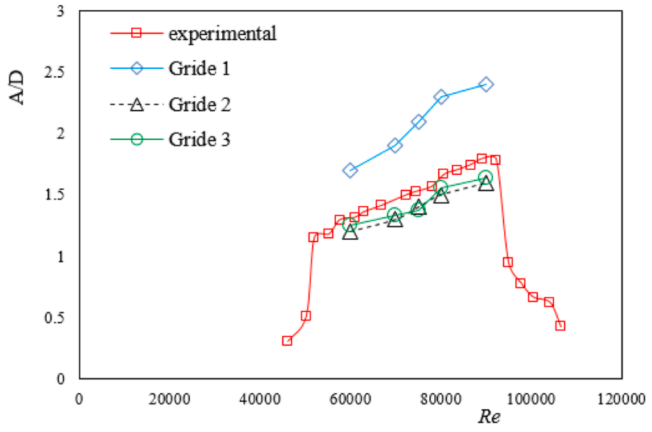

Fig. 5. Independent resolution of gridding.

Table 3
Specifications of the oscillator system.

Relative mass	m^*	94/0، 89/1
Relative attenuation for energy inhibition	ζ	0، 08/0، 16/0
Oscillating mass	*m (kg)*	75/10، 375/5
Straightforward	*D (m)*	0889/0
Strength coefficient of spring	*K (N/m)*	1200, 1000, 800, 400, 1600

analysis of vortexes of a rigid cylinder of a degree of freedom with abrasive support in the Re interval is between 30,000 and 130,000. The simulation environment of the oscillator system for the vibrations caused by vortices is shown in Fig. 6. For this simulation, two springs installed at both ends of the cylinder have been used.

In general, the governing equations of numerical software are based on Navier-Stokes equations. These equations are valid in slow and turbulent flows and for an incompressible and Newtonian fluid in three dimensions that is under the influence of gravitational forces, it is written as follows:

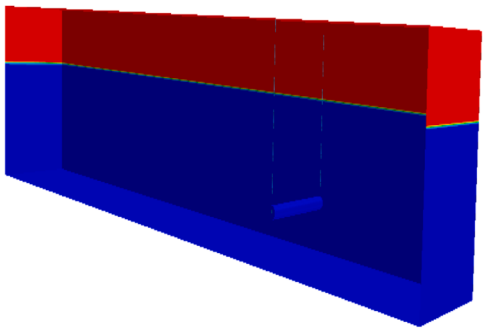

Fig. 6. The simulation environment of the oscillator system.

$$\frac{\partial U_i}{\partial x_i} = 0 \tag{1}$$

$$\frac{\partial U_i}{\partial t} + U_j\frac{\partial U_i}{\partial x_j} = -\frac{1}{\rho}\frac{\partial P}{\partial x_i} + \nu\frac{\partial^2 U_i}{\partial x_j \partial x_j} + g_i \tag{2}$$

The simulations are performed under defined physical conditions. In this case, the amount of pressure and velocity of the fluid can be decomposed in the form of Eqs. (3) and (4):

$$U_i = \overline{U}_i + u_i \tag{3}$$

$$P = \overline{P} + p \tag{4}$$

In this equation, $\overline{P}$ and $\overline{U}_i$time average are pressure and velocity, and p and u are fluctuating values of fluid velocity and pressure. By inserting Eqs. (3) and (4) into the Navier-Stokes equation, the average Reynolds Navier-Stokes equation will be created in the form written in Eqs. (5) and (6).

$$\frac{\partial \overline{U}_i}{\partial x_i} = 0 \tag{5}$$

$$\frac{\partial \overline{U}_i}{\partial t} + \overline{U}_j\frac{\partial \overline{U}_i}{\partial x_j} = \frac{1}{\rho}\frac{\partial \overline{P}}{\partial x_i} + \nu\frac{\partial^2 \overline{U}_j}{\partial x_j \partial x_j} - \frac{\partial \overline{u_i u_j}}{\partial x_j} + g_i \tag{6}$$

It should be noted that the ensemble average of the Navier-Stokes equations (RANS) is very similar to the Navier-Stokes equations and only the Reynolds stress tensor term ($\overline{u_i u_j}$) has been added to it. If the Reynolds stress is added to the Navier-Stokes equation, the RANS equations define the flow characteristics as a time average. One of the common methods to calculate the Reynolds stress tensor value is to use Bausins' point of view. In this method, the stress tensor is defined from Eq. (7) as a function of dynamic viscosity:

$$-\overline{u_i u_j} = \nu_t\left(\frac{\partial \overline{U}_i}{\partial x_j} + \frac{\partial U_j}{\partial x_i}\right) - \frac{2}{3}k\delta_{ij} \tag{7}$$

In this equation, δ_{ij} is the cranker's delta, whose value is considered to be 1 in the condition i = j and 0 at other times. Also, k is the kinetic energy of the turbulent flow, which is calculated from the Eq. (8):

$$k = \frac{1}{2}\overline{u_i u_i} \tag{8}$$

RANS equations can be solved by calculating the turbulent viscosity. In the simulations carried out in this study, the K-epsilon model was used. In this method, using Eq. (9), the viscosity of the mixture can be calculated as:

$$\nu_t = C_\mu\frac{k^2}{\varepsilon} \tag{9}$$

In this equation, the values of k and ε are calculated using the equations of motion (10) and (11).

$$\frac{\partial k}{\partial t}+\frac{\partial}{\partial x_j}(k\overline{U}_i)=\frac{\partial}{\partial x_j}\left[\left(\upsilon+\frac{\upsilon_t}{\sigma_k}\right)\frac{\partial k}{\partial x_j}\right]+p_k-\varepsilon \tag{10}$$

$$\frac{\partial \varepsilon}{\partial t}+\frac{\partial}{\partial x_i}(\varepsilon\overline{U}_i)=\frac{\partial}{\partial x_j}\left[\left(\upsilon+\frac{\upsilon_t}{\sigma_\varepsilon}\right)\frac{\partial \varepsilon}{\partial x_j}\right]+\frac{\varepsilon}{k}(C_{\varepsilon 1}P_k-C_{\varepsilon 2}\varepsilon) \tag{11}$$

$C_{\varepsilon 1}$,$C_{\varepsilon 2}$, σ_k,σ_ε, CK values are constant and the PK value is created under the influence of perturbed kinetic energy and is calculated from Eq. (12),

$$P_k=-\overline{u_i u_j}\frac{\partial \overline{U}_i}{\partial x_j} \tag{12}$$

To model the free surface, it is necessary to evaluate the interaction between two fluids, water and air. In the volume of fluid (VOF) method, each phase in the free surface is expressed by introducing the parameter α. If there is only one phase of the fluid in the target cell, the α value is considered 0 or 1 and the Navier-Stokes equations are solved for the above fluid. Also, if there are two fluid phases in a cell, the value of α will be between 0 and 1. In this condition, the density and viscosity of the cell are calculated according to the volume percentage of each fluid, as the average characteristic of both fluids from Eqs. (13) and (14).

$$\rho=\alpha\rho_1+(1+\alpha)\rho_2 \tag{13}$$

$$\nu=\alpha\nu_1+(1+\alpha)\nu_2 \tag{14}$$

As a result of the impact of the water flow with the specified speed on the cylinder under the water surface, the cylinder will move. According to the degrees of freedom defined for the Vivas vortex converter, the cylinder will only be able to oscillate along the vertical axis. In this condition, the equation of cylinder movement is expressed as Eq. (15):

$$m\ddot{z}+C_{tot}\dot{z}+Kz=F_y \tag{15}$$

In this equation, m represents the mass of the oscillator system, which is calculated from Eq. (16).

$$m=\frac{1}{3}m_s+m_c \tag{16}$$

According to Eq. (16), the mass of the oscillator system consists of the total mass of the cylinder and the considered springs around it. In this equation, ms is the mass of each spring and mc is the mass of the cylinder. In Eq. (15), k is the stiffness coefficient of the springs that are placed parallel on the sides of the cylinder. Because the springs are parallel, the total stiffness coefficient will be calculated from the sum of the stiffness coefficients of each spring. It should be noted that in this problem, the stiffness coefficient of the two considered springs is equal, and thus the value of k is twice the stiffness coefficient of each of the springs. The other term in Eq. (15), C is the damping coefficient of the spring, which can be calculated from Eq. (17).

$$C_{tot}=C_{structure}+C_{harness} \tag{17}$$

According to Eq. (17), the damping of the entire embedded oscillator system consists of the sum of the losses caused by the power transfer to the oscillator system and the internal resistance of the generator when converting mechanical energy to electrical energy.

Some of these variables are evaluated on the operation of the vibration system due to unsteady fluid force. These performances are carried out for relative masses of 1.89 and 0.49, and the effects of the Re on the relative amplitude of the cylinder on different dampers and springs are considered. To calculate the relative amplitude, an average of at least 15 ranges of motion has been used. The Re is considered to be between 30,000 and 130,000 to evaluate the vibrational system function.

3. Results and discussion

The results of the simulation of the oscillator system are validated with valid laboratory results. Subsequently, by changing the system parameters, including spring hardness coefficient, relative mass, and damping coefficient, the effect of these factors on the range of maximum and minimum frequencies has been investigated. Ultimately, the design and construction of a wave energy converter that can be tested on the sea is done. Some of the variables investigated are evaluated on the operation of the vibration system due to vortices. These performances are carried out for relative masses of 1.89 and 0.49, and the effects of the Re on the relative amplitude of the cylinder on different dampers and springs are considered (Table 4). To calculate the relative amplitude, an average of at least 15 ranges of motion has been used. The Re is considered to be between 30,000 and 130,000 to evaluate the vibrational system function.

The value of the cylinder movement range is calculated from the average of at least 15 domains of the system's total time history. Fig. 7 shows the amplitude range of the oscillator system with a hardness factor of 400 N / m. The horizontal axis of the diagram, the Re dimensional number, and the vertical axis show the relative dimensionless number. From the 100,000 Re, the range of motion can be assumed to be relatively constant, although slight variations are visible in the graphs. In Table (4), the maximum and minimum in the three branches range of the cylinder movement in all three modes of relative damping is shown in the experimental results.

In this case, the K value has been increased to 1000 N/m (Table 5). The results of this state are shown in Fig. 8. The process of variation of the results is compared with the results of Lee et al. [3]. As before, by increasing the Re, the cylinder motion rises. This amount increases to a certain speed. In the case of a cylinder without a damping factor, the relative amplitude of the cylindrical movements is maximal.

The stiffness coefficient was also increased to 1600 N/m. The results in Fig. 9 show that the amplitude of the cylindrical motion is lower than that of the previous ones by increasing the stiffness coefficient of the spring. However, as in the previous states, the amplitude of the oscillations decreases with increasing relative slope. In this section, data from the previous section have been used and the effect of spring stiffness on a constant relative damping is investigated. As the spring hardening coefficient increases, the cylinder fluctuation range is higher in Re. For this reason, the amplitude of the cylindrical oscillations in higher Re is increased by increasing the stiffness coefficient of the spring.

This increase in a range up to 1200 N / m is continued, and this amount is further reduced by increasing the hardness of the spring. It is important to study these relative masses for the spring hardness coefficients, as presented in the following figures (9–12). According to experiments conducted by Vikestad [31], in partial masses smaller than 0.54, the lower branch of the vibrations caused by vortices is eliminated and vibrations occur with a very large amplitude.

In this case, the stiffness coefficient has been increased to 800 N/m. By increasing the hardness of the spring, the difference between the two relative mass diagrams is increased compared to the previous one. In the low Re, with an increase in relative mass, the relative range of the mean increases slightly. This trend continues to Re 50,000, after which relative weight reductions increase the relative amplitude. The transition from the primary branch to the high branch of the relative masses is less likely to occur later. At the end of the Re interval, for larger relative masses, the transition occurs earlier, and the response lies in the lower branch of vibrations caused by vortices. In the relative damping state, the relative range of the mean has increased with decreasing relative mass. In this case, by decreasing relative mass, the interval in which the relative amplitude is significant is larger, and the place where it occurs is transmitted to larger Re. The spring hardness factor has been increased to 1600 N / m. In this case, the difference between two relative masses in a relative zero damping ratio has decreased, and in partial relative damping, the relative amplitude increased slightly. The relative amplitude of the mean relative to the previous state has decreased for both relative masses. The relative amplitude of the mean relative to the

Table 4
Average relative amplitude for K = 400 N / m.

		Initial excitation branch			Upper branch			Lower branch		
ζ	U (m/s)	Min. $A_{ave.}/D$ (present method	Min. $A_{ave.}/D$ (exp	Error (%)	Max. $A_{ave.}/D$ (present method)	Max. $A_{ave.}/D$ (exp.)	Error (%)	Min. $A_{ave.}/D$ (present method	Min. $A_{ave.}/D$ (exp.)	Error (%)
0	59/0	0.36	0.46	21.7	25/1	.36/1	8	0.42	0.47	10.6
08.0	59/0	0.27	0.34	20.5	95/0	09/1	13	0.2	0.36	44.4
16/0	59/0	0.23	0.34	32.3	68/0	776/0	12	0.12	0.32	62.5

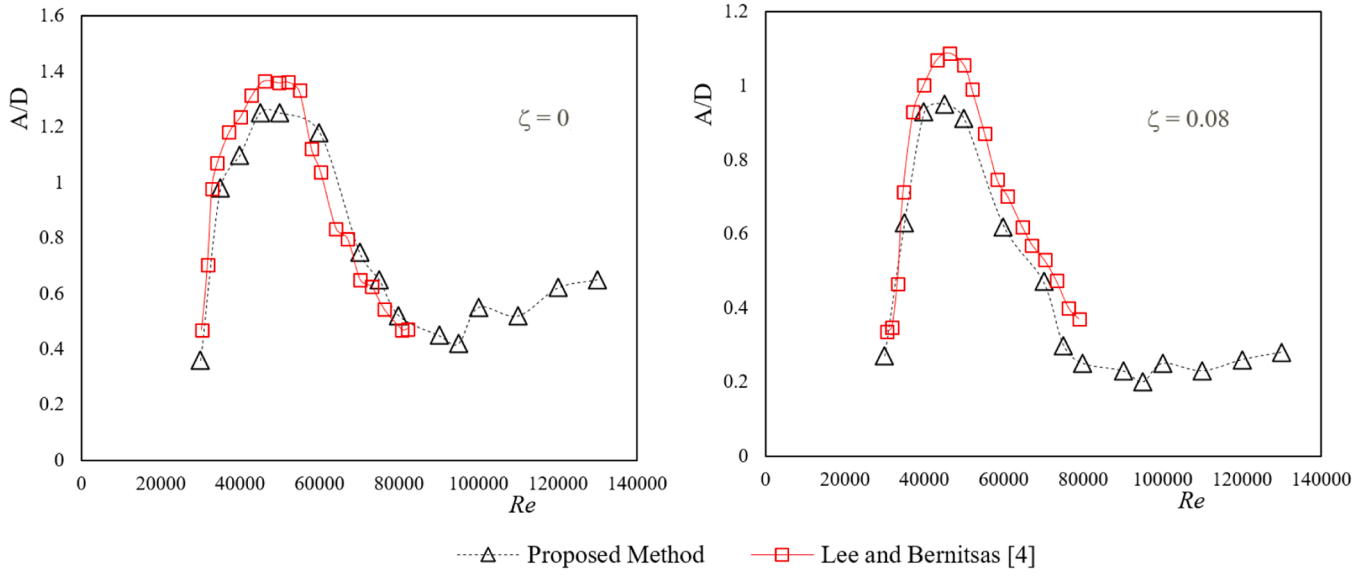

Fig. 7. The mean relative amplitude for the vibrational vibration system for K = 400 N / m and m * = 1.89 for ζ = 0 and ζ = 0.08.

Table 5
Average relative amplitude for K = 1000 N / m.

		Initial excitation branch			Upper branch			Lower branch		
ζ	U (m/s)	Min. $A_{ave.}/D$ (present method	Min. $A_{ave.}/D$ (exp	Error (%)	Max. $A_{ave.}/D$ (present method)	Max. $A_{ave.}/D$ (exp.)	Error (%)	Min. $A_{ave.}/D$ (present method	Min. $A_{ave.}/D$ (exp.)	Error (%)
15	0.73	0.62	13	. 73/1	5/1	63	0.33	0.12	1.1	0
0.13-	0.51	0.58	8	34/1	23/1	70	0.24	0.07	04/1	08/0
2.2-	0.43	0.44	14	99/0	85/0	81	0.19	0.035	89/0	16/0

previous state has decreased for both relative masses. Therefore, for a hardness factor of 1200 N / m2, it has the largest relative oscillation range and the widest upper branch of vibration caused by vibrations. Although the relative range was expected to increase with decreasing relative mass, however, the behavior of branches of vibrations caused by vortices and the extent of each branch was not predictable for any coefficient of hardness and damping. For the design of the energy converter system, it is important to have detailed information on the relative amplitude and range of Re in which the system operates at maximum efficiency. To better understand the cylinder simulation for oscillations due to vortices, the flow lines from the cylinder for a period of motion are shown in Fig. 10.

The flow through the cylinder in the interval from time to time, according to the vertex, moves the cylinder upwards and moves the cylinder to the bottom in the other interval. The flow lines after the cylinder have a different formation that indicates the vertices released after passing through the cylinder. In Fig. 10, the flow lines in Mode 1, from below to the cylinder move the cylinder upwards. His movement continues until the 4th stage reaches its maximum range, then in mode 5, the flow will be taken and the flow lines will flow through the cylinder and the cylinder will move downwards. This oscillation cycle caused by the vertex causes the cylinder to be raised and lowered in a regular cycle. By connecting the cylindrical movements to an energy conversion generator, cylindrical oscillations of the electric power can be generated. Making the conditions that can give us the greatest range of motion will make this energy converter have the best returns. Even if it is high, it can be used to pump seawater for a water purifier to better understand the movements of the cylinder caused by vortices, in this section the generated vortices caused by flow through the cylinder are shown in Figs. (11) and (12) for a coefficient of spring hardness of 800 and 1200 N / m, and Relative zero attenuation is displayed. Research shows that the transition from one branch to the other branch causes the cylindrical displacement history to not be uniform and changes in summers in succession [32].

The mechanism of the vortex is one of the vortices around the base grows which is larger than the other vortex (Fig. 13). The larger vortex is strong enough to drag its opposite vortex (vortex B) along the trajectory region. The circle in vortex A is done in the clockwise direction, while in vortex Â B it is in the opposite direction of the clockwise motion. Finally, at a moment, the vortex A flows and turns into a vortex and flows through the flow downstream. This procedure continues until a new vortex flows on one side of the cylinder and these flows lead to the

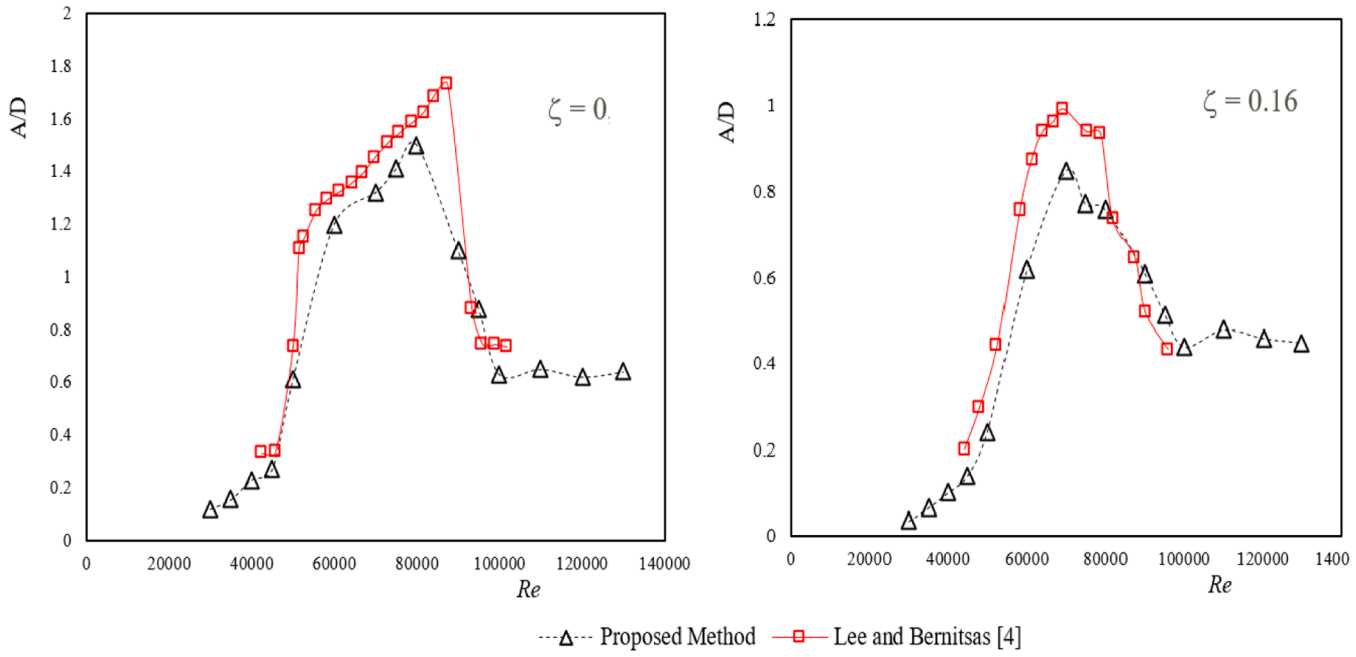

Fig. 8. Average relative amplitude for the vibrational vibration system for K = 1000 N / m and m * = 1.89: ζ = 0, and ζ = 0.16.

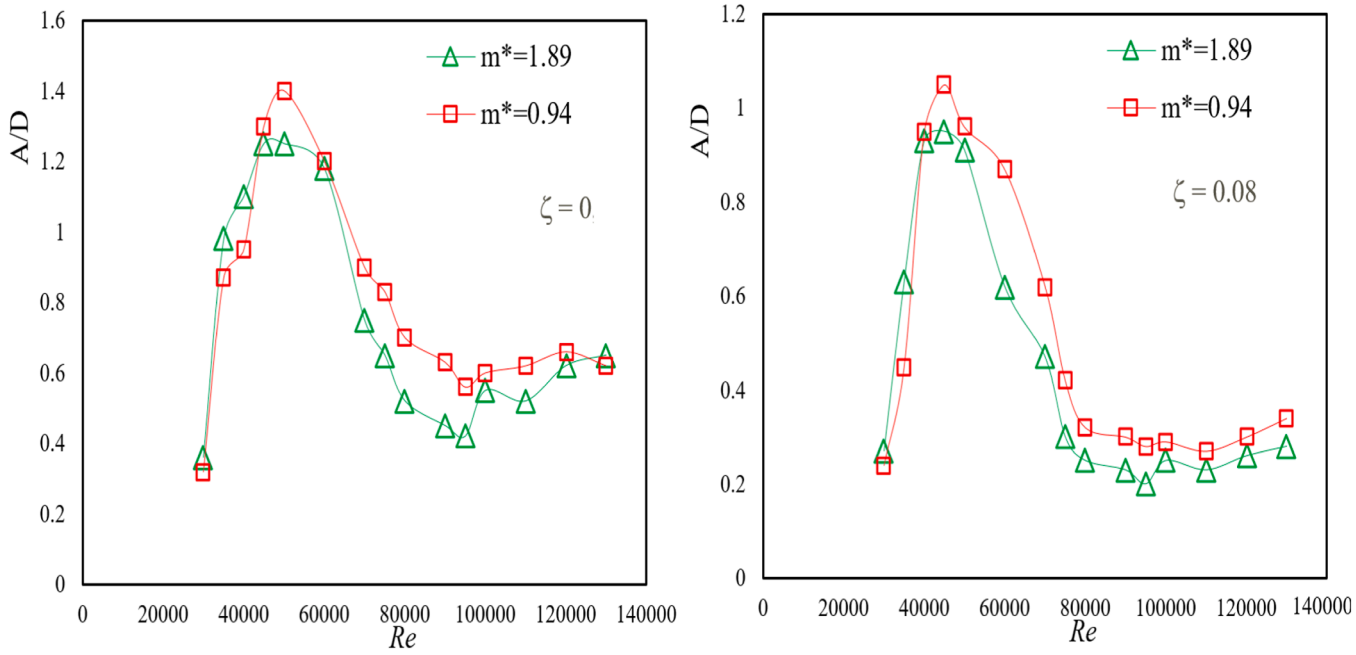

Fig. 9. Average relative amplitude for the vibrational vibration system for K = 400. N / m: a) ζ = 0, b) ζ = 0.08.

continuity of the alternating behavior between the two sides of the cylinder.

Research shows that the transition from one branch to the other branch causes the cylindrical displacement history to not be uniform and changes in summers in succession. Research shows that the transition from one branch of the response to another makes the time history of the displacement of the cylinder not uniform and the value of the peaks changes in successive fluctuations. Also, the vortex burst pattern is not stable during the transition period. In the simulations, after the initial time of the cylinder movement, the time history of the cylinder movement is almost uniform and the flow pattern is stable, so the curtain curve is shown for a period of motion. In this section, Cantor Virtuosity is presented in a different hardness factor. These shapes are shown for the Re of 90,000. The vortex is shown for a cylinder movement period.

To further understand the formation of vortices around the cylinder, the hardness coefficient has been increased to 1200 N / m. The shape of the vortex for the Re of 90,000 is shown in Fig. 11. As in the previous case, the vortex pattern in this run follows a similar trend. In comparison with the previous state, the vortexes deposited at the end of each oscillation period give less penetration into the field. Staying stable The vortex shrinkage pattern can indicate the completion of the transition phase and the positioning of the response in the upper branch of vibrations caused by vortices.

The presence of a body causes the formation of vortices on both sides

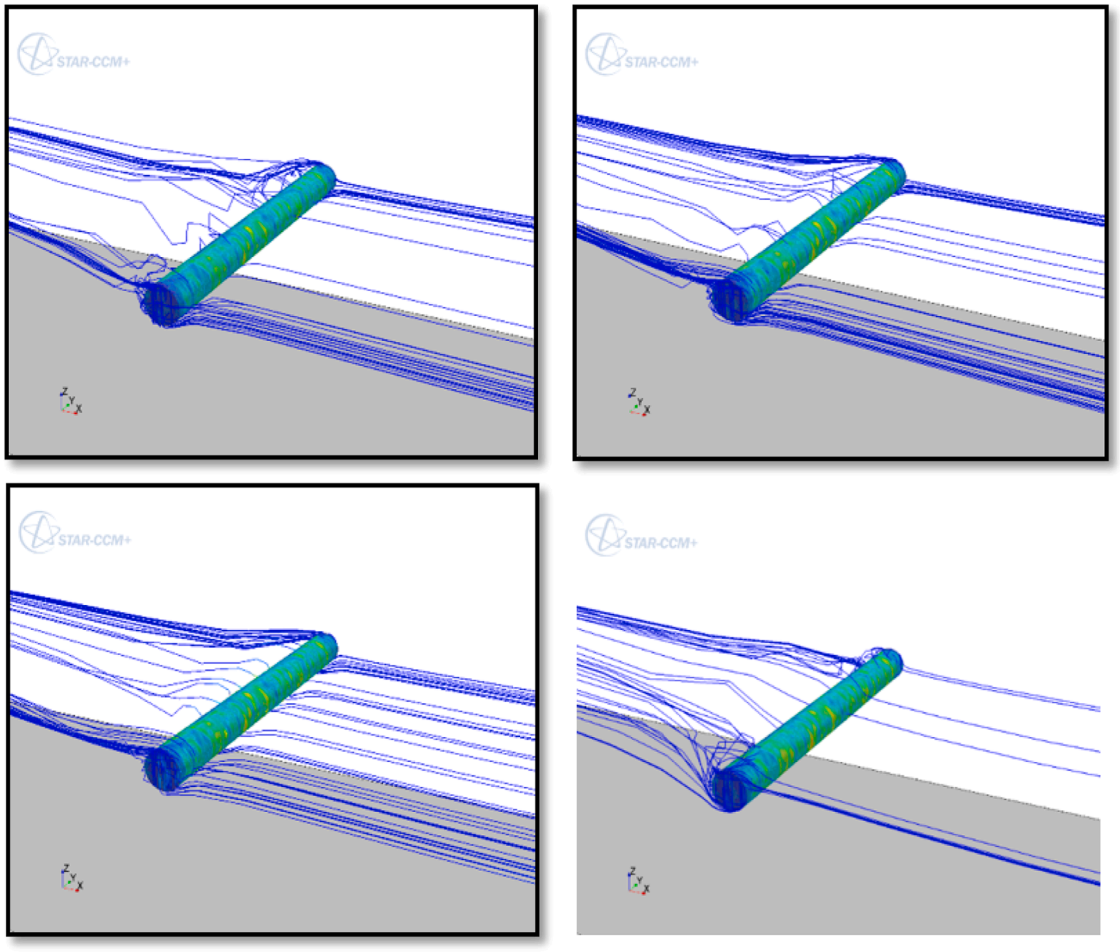

Fig. 10. The formation of flow lines caused by passing through a cylindrical surface.

of the cylinder, and then they are released in the field of flow. Considering that the purpose of this study is to simulate the VIVA converter in the software in the first stage. Then, proceeding with the consideration of the results of studying various factors using numerical solutions, designing and constructing a vortex converter will be done. In this study, using two-dimensional computational fluid dynamics, the vibrations of a rigid cylinder flow of a degree of freedom with an elastic support were investigated. For this purpose, in the StarCcm software, the experimental conditions of the Vivac converter have been simulated and the method of setting the parameters necessary to verify the converter in the software has been done. To simulate vibrations caused by vortices, the K-Epsilon turbulence model is used. Validation of the numerical model presented with Laboratory results by Lee et al. [3] have been compared. It was also shown that the maximum relative amplitude of the cylinder for a spring with a coefficient of hardness of 1200 n / m and a relative slope of zero and a relative mass of 94 in Re is 90,000, 75/1.

Considering that turbulent flow equations are used in this simulation. RANS equations can be solved by calculating the turbulent viscosity. In general, there are two methods to calculate the viscosity of the mixture: 1) Ka-Omega method, and 2) Ka-Epsilon method. In each of the two methods, the amount of turbid viscosity will be calculated using the equations of motion. Considering that turbulent flow equations are used in this simulation. At low Re, the flow is laminar and will turn into turbulent flow as the velocity increases. However, most currents in nature are turbulent. Therefore, in this research, the Ka-Epsilon type turbulent flow model has been used, the governing equations of which will be described below.

To model the free surface, it is necessary to evaluate the interaction between two fluids, water and air. In the volume of fluid (VOF) method, each phase in the free surface is expressed by introducing the parameter α. If there is only one phase of the fluid in the target cell, the α value is considered 0 or 1 and the Navier-Stokes equations are solved for the above fluid. In this research, the basic characteristics of the numerical setup used to simulate the VIVACE wave converter were stated. At first, the specifications of the computational domain, such as the dimensions of the domain, boundary conditions, and the location of the cylinder in the domain, were discussed. Then the physics governing the flow, fluid characteristics in the domain, time step, and other physical characteristics were presented in detail.

It was shown that by decreasing relative mass, the transition from the response branches to vibrations caused by the flow and vibrations caused by vortices in larger Re, in other words, occurs later, and the stable branches respond more broadly and the peak of the relative amplitude of the vibrations caused by vortices will be higher and its location will be larger than the larger Re. It was also shown that the maximum relative amplitude of the cylinder for a spring with a coefficient of hardness of 1200 n/m a relative slope of zero and a relative mass of 94 in Re is 90,000, 75/1. To design a V / V converter without considering The natural constraints of the best possible design the one that can work in a wider range and with more efficiency.

In this research, the preliminary was used to simulate the waveform transducer. Initially, computational domain characteristics, such as domain dimensions, boundary conditions, and positioning of the cylinder in the domain, were introduced. Then, the governing physics of flow, the fluid properties of the domain, the time step, and other physical properties were presented accurately. Given the physical conditions

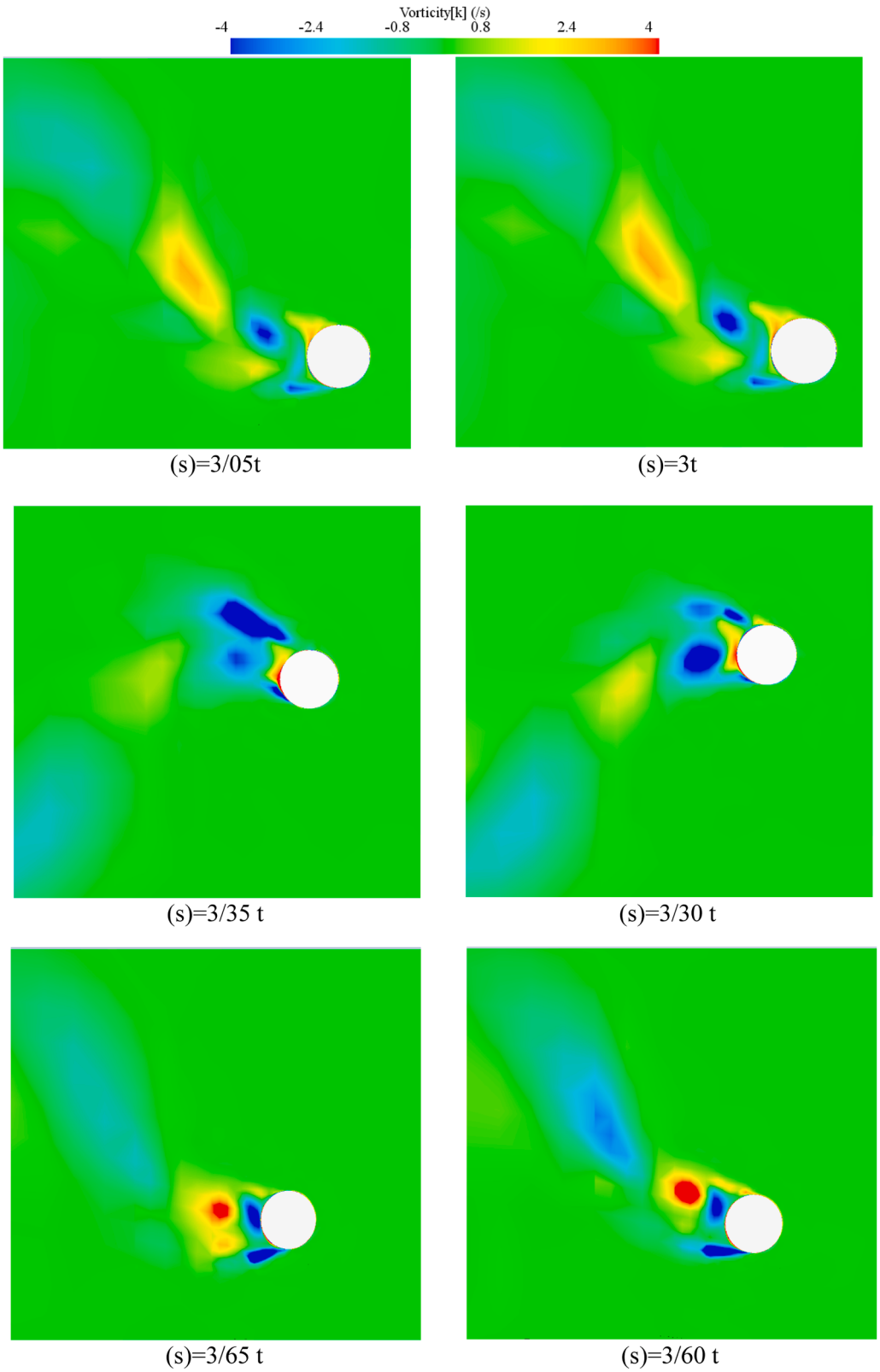

Fig. 11. The formation of vortices around a cylinder due to the flow through a spring tensile strength of 800 N / m, $\zeta = 0$, m * = 1.89, and a Re of 90,000.

applied in the computational range, the equations governing the flow physics are described separately.

The main goal of this study is to obtain the maximum efficiency of the energy converter due to the formation of vortices and the development of the range of converter functions. According to previous studies, maximum system efficiency occurs when vibrations are caused by vortices. For this reason, the simulation of a cylinder was selected in the range of Re. According to the predictions based on the references, in order to increase the efficiency and range of the functional point of the converter under vibrations caused by vortices, a range of spring

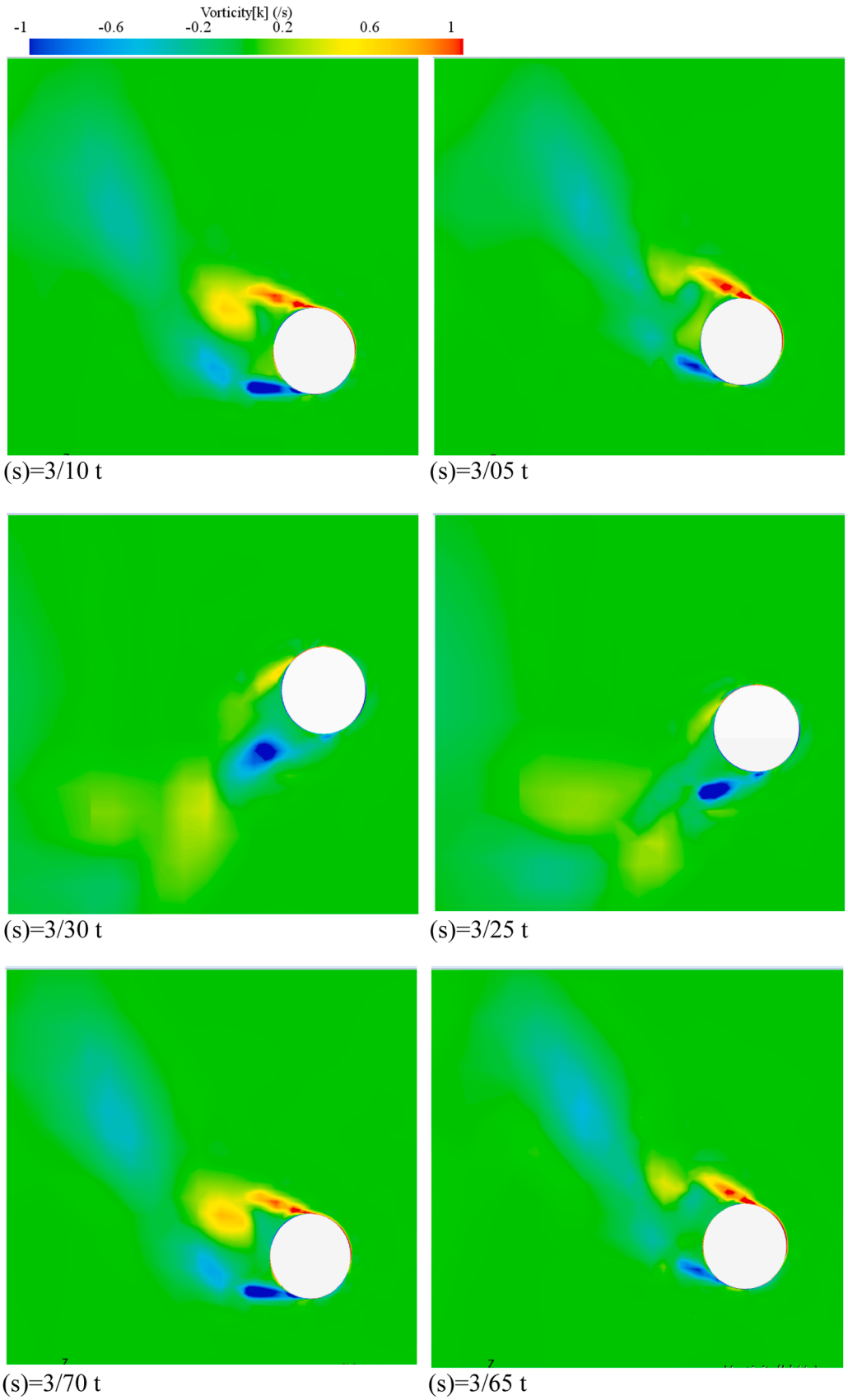

Fig. 12. The formation of vortices around a cylinder due to flow throughput at 1200 N / m, $\zeta = 0$, m * = 1.89 and Re of 90,000.

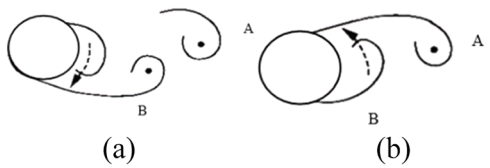

Fig. 13. The vortex flow mechanism. Before vortex A flows, vortex B is drawn along the trail; b) the vortex is drawn along the trail before the vortex B is flowing.

hardness coefficient, damping coefficient, and relative mass were selected.

In the following, the vibrations caused by vortices for a rigid cylinder of a degree of freedom with an elastic support were investigated. The simulation performed with great precision shaped the motion of the cylinder caused by flow vortices. The simulations in the Re range from 30,000 to 130,000. With variation in spring hardness coefficient, relative damping, and relative mass, the cylindrical performance was investigated in different Re and compared with laboratory results, and a fairly good accuracy was obtained. The simulation was targeted and optimized and the following results were obtained: with the increase in the stiffness coefficient of the spring, the oscillation amplitude has increased, but this increase in amplitude is transmitted to larger Re. In the relative mass range, the relative amplitude increases with relative mass degradation. The relative peak value for lower relative masses is transmitted to larger Re. By reducing relative mass, the range of Re in which the phenomenon of synchronization occurs is wider and consequently extends to a range of Re in which the relative amplitude is large. Find out The maximum relative amplitude of the cylinder in the simulations of this chapter for a spring with a hardness factor of 1200 n/m and a relative slope of zero and a relative mass of 94 in the Re is 90,000, 1.75. Also, the formation of a vortex burst pattern is displayed so that its use can help to better understand the phenomenon. Since the time histories of average relative amplitude under specific conditions may take a long to analyze, in future studies it can be addressed.

In summary, the convergence of the mesh was investigated to determine the optimal mesh size for accurate simulation results. Three different mesh sizes, comprising 301,223, 474,344, and 646,321 cells, were tested to evaluate the impact on solution accuracy. The results showed that increasing the number of cells from 301,223 to 474,344 significantly enhances the accuracy of the solution, reducing the error when compared to experimental results. However, further increasing the number of cells to 646,321 does not lead to a substantial improvement in accuracy, indicating that the solution has converged at this mesh density. This observation highlights that while finer meshes can improve accuracy, they also significantly increase computational costs. The trade-off between accuracy and computational efficiency must be carefully considered, especially for large-scale simulations.

The VIV was conducted on a rigid cylinder with one degree of freedom, supported by an elastic foundation, within a Reynolds number range of 30,000 to 130,000. The results demonstrated that as the Reynolds number increases, the cylinder's motion becomes more pronounced, peaking at a certain Re value before stabilizing. This behavior is consistent with the classic VIV response, where the flow-induced forces resonate with the natural frequency of the structure, leading to large amplitude oscillations. The influence of various parameters, including the spring stiffness coefficient, relative mass, and damping ratio, on the VIV response was systematically investigated.

The study further explored the effects of relative mass and damping ratio on the VIV response. It was seen that lighter structures are more susceptible to fluid-induced forces, leading to more significant displacements. Similarly, the damping ratio played a crucial role in controlling the amplitude of oscillations. As damping ratio increased, the energy dissipation in the system increased, leading to a reduction in the oscillation amplitude. This trend is evident, where the flow lines indicate a more stable vortex shedding pattern at higher damping ratios. The presence of damping not only reduces the oscillation amplitude but also stabilizes the flow pattern.

The detailed analysis of the VIV system provided valuable insights for the design and optimization of wave energy converters. The findings suggest that for a VIV-based energy converter to operate at maximum efficiency, the system parameters, including spring stiffness, relative mass, and damping, must be carefully optimized to match the expected flow conditions. The study shows that a spring stiffness coefficient of 1200 N/m offers the largest oscillation range and the broadest upper branch of vortex-induced vibrations, making it an ideal choice for energy harvesting applications. In practical terms, the results suggest that by optimizing the stiffness and damping of the system, it is possible to enhance the energy extraction efficiency of VIV-based converters.

Fy likely represents the vertical force acting on the cylinder due to the fluid flow. In VIV, this force is primarily caused by the periodic shedding of vortices from the cylinder's surface. The K-Epsilon turbulence model was employed to simulate the flow-induced vibrations in this study. The model's effectiveness in capturing the complex flow phenomena, such as vortex shedding and turbulent wake formation, was validated by comparing the simulation results with the experimental data from Lee et al.. The model successfully reproduced the key characteristics of the flow, including the transition from laminar to turbulent flow at higher Reynolds numbers, as indicated in the validation results. The choice of the K-Epsilon model was based on its robustness and widespread use in simulating turbulent flows in engineering applications. However, it is important to note that while the model provides a good approximation of the flow behavior, further refinement, such as using Large Eddy Simulation (LES) or Direct Numerical Simulation (DNS), could offer more detailed insights, especially in capturing the fine-scale vortex structures.

In this study, numerical simulation was used to check the performance of Vivas energy converter. In general, numerical methods have advantages compared to other methods. Considering that the number of influencing parameters on such a converter is large, the application of numerical methods gives the researcher the power to change different parameters. However, the special limitation is the lack of access, there is no suitable laboratory to check such a system, or its specifications are limited, and there is a possibility of damage to the laboratory converter at high speeds. Furthermore, the model has only been checked in one degree of freedom. By using numerical methods, the behavior of the Vivas converter system can be predicted in the real environment, and by using the results of the numerical method, the real model can be checked and designed. In future the study can be extended to study the energy conversion efficiency of VIVACE model.

4. Conclusion

In conclusion, this study explored into the novel approach of harnessing energy from fluid flow-induced vibrations, presenting a comprehensive investigation into the dynamics surrounding this innovative method. In this research, numerical simulation was used to evaluate the performance of the VSD converter. Using numerical methods allows the researcher to change the parameters. Through detailed simulations using the K-Epsilon turbulence model, it was found that increasing the number of mesh cells significantly improves solution accuracy up to a certain point, beyond which further refinement yields diminishing returns. On the other hand, there is no proper laboratory for examining such a system and its specifications are limited and at high speeds, there is a potential for damage to the laboratory transducer. By using numerical methods, we can predict the behavior of the VS converter system in the real environment and use the results of numerical methods to investigate and design the real model. The purpose of this study was to investigate the ability of computational fluid dynamics to simulate the VOA system and examine various parameters on this converter. The data can be used numerically for optimal design. The second

part examines the physical model of the VIVACE converter. Then governing equations for fluid dynamics and the rigid body motion equation were presented. Then, the domain of solution, boundary conditions, and selected computational grids were investigated. The investigation into the effects of varying spring stiffness and relative mass on the amplitude and frequency of cylinder oscillations highlighted key factors influencing the efficiency of wave energy converters. This section examines the solvability of the computational grid for the cylinder. After that, the vibrations of a vortex of a rigid cylinder of a degree of freedom with elastic support in the Re were investigated between 30,000 and 130,000. The data obtained from the simulation was compared with the reported values from experiments conducted at the University of Michigan University. It was observed that increasing the stiffness coefficient initially leads to an increase in the amplitude of oscillations, but beyond a certain threshold, the oscillations begin to decrease. Additionally, the study showed that the relative mass significantly impacts the transition between different branches of vibrational response, with smaller masses delaying this transition and broadening the stable response range.

The numerical results, validated against experimental data showed a strong correlation, particularly for a spring stiffness of 1200 N/m, zero damping, and a relative mass of 1.89. Under these conditions, the maximum relative amplitude of the cylinder reached 1.75 at Re 90,000. The implications of these findings underscore the viability and promise of this energy extraction method, particularly in harnessing energy from fluid flows that were traditionally deemed unsuitable for such applications. Additionally, the study revealed that increasing the spring stiffness up to 1200 N/m enhanced the oscillation amplitude, but further increases led to a reduction. The impact of damping and relative mass was also significant, with lower relative masses and damping ratios resulting in larger amplitude oscillations across a broader range of Re. For instance, with K = 400 N/m and zero damping, the minimum and maximum relative amplitudes in the upper branch were 0.36 and 1.36, respectively, with errors of 21.7 % and 8 % compared to experimental values. With increased stiffness (K = 1000 N/m), the maximum relative amplitude was 1.73, with a reduced error of 13 %. The findings suggest that optimal VIV performance for energy conversion applications is achieved with a spring stiffness of around 1200 N/m, zero damping, and a relative mass close to 1.89, within the studied Re range.

To generate electricity and connect the device to the generator, the linear movement of the cylinder must first be converted into rotary movement. Considering the condition of the device in the sea, it is important to use a mechanism that can perform this movement conversion. Then the research will continue to improve the converter so that automatic measuring devices can be installed on the converter. This research will be done on improving the transducer in order to automatically record the sea data at any moment and display the necessary calculations according to the range of the cylinder movement. Due to the lack of measuring devices, the design and construction of the measuring device is on the path of evolution of this energy converter so that it can be used to take online data from the converter. After the completion of the construction and testing process of the converter in the sea, a field of this converter will be operated side by side in compliance with environmental laws. The output power from the converter will be used to pump seawater.

Overall, this research provides valuable insights into optimizing the design of vortex-induced vibration-based energy converters. The findings underscore the importance of selecting appropriate system parameters, such as mesh size, spring stiffness, and relative mass, to achieve maximum efficiency in energy conversion. The validated simulation results lay the groundwork for future experimental studies and the practical implementation of wave energy converters in real-world marine environments.

5. Statements and declarations

5.1. Institutional review board statement

Not Applicable

5.2. Informed consent statement

Not Applicable.

5.3. Data availability statement

Not applicable.

CRediT authorship contribution statement

Zahrapanah Razaviyn: Resources, Project administration, Methodology, Formal analysis, Data curation, Conceptualization. **Milad Heidari:** Investigation, Funding acquisition, Formal analysis, Data curation, Conceptualization. **Sivasakthivel Thangavel:** Resources, Investigation, Formal analysis. **Vikas Verma:** Methodology, Investigation, Formal analysis. **Ashwani Kumar:** Writing – review & editing, Writing – original draft, Visualization, Formal analysis. **Ashok Kumar Yadav:** Writing – review & editing, Writing – original draft, Resources.

Declaration of competing interest

The authors declare no conflict of interest.

Data availability

Data will be made available on request.

References

[1] M.M. Bernitsas, K. Raghavan, Fluid motion energy converter, U.S. Patent 7,493,759, February 24, 2009.
[2] R. Kamaldev, Energy Extraction from a Steady Flow Using Vortex Induced Vibration, Michigan University, 2007. PhD thesis.
[3] J.H. Lee, M.M. Bernitsas, High-damping, High-Reynolds VIV tests for energy harnessing using the VIVACE converter, Ocean Eng. 38 (16) (2011) 1697–1712.
[4] C.C. Chang, Hydrokinetic Energy Harnessing By Enhancement of Flow Induced Motion using Passive Turbulence Control, University of Michigan, Ann Arbor, 2010. Ph.D Thesis.
[5] M.M. Bernitsas, K. Raghavan, G. Duchene, Induced Separation and Vorticity Using Roughness in VIV of Circular Cylinders at 8103 Re 1.5105, in: *Proceedings of the International Conference on Offshore Mechanics and Arctic Engineering*–OMAE, 2008.
[6] B. Zhou, J. Hu, P. Jin, K. Sun, Y. Li, D. Ning, Power performance and motion response of a floating wind platform and multiple heaving wave energy converters hybrid system, Energy 265 (2023) 126314, https://doi.org/10.1016/j.energy.2022.126314.
[7] J.T. Klamo, A. Leonard, A. Roshko, The effects of damping on the amplitude and frequency response of a freely vibrating cylinder in cross-flow, J. Fluids. Struct. 22 (6) (2006) 845–856.
[8] N. Jauvtis, C.H.K. Williamson, Vortex-induced vibration of a cylinder with two degrees of freedom, J. Fluids. Struct. 17 (7) (2003) 1035–1042.
[9] R. Govardhan, C.H.K. Williamson, Resonance forever: existence of a critical mass and an infinite regime of resonance in vortex-induced vibration, J. Fluid. Mech. 473 (2002) 147–166.
[10] K. Vikestad, J.K. Vandiver, C.M. Larsen, Added mass and oscillation frequency for a circular cylinder subjected to vortex-induced vibrations and external disturbance, J. Fluids. Struct. 14 (7) (2000) 1071–1088.
[11] B. Zhou, K. Ding, J. Wang, L. Wang, P. Jin, T. Tang, Experimental study on the interactions between wave groups in double-wave-group focusing, Phys. Fluids 35 (3) (2023) 37118, https://doi.org/10.1063/5.0142042.
[12] L. Yin, L. Wang, B.Z. Keim, K. Konsoer, Z. Yin, M. Liu, W. Zheng, Spatial and wavelet analysis of precipitation and river discharge during operation of the Three Gorges Dam China, Ecol. Indic. 154 (2023) 110837, https://doi.org/10.1016/j.ecolind.2023.110837.
[13] M. Yang, Y. Wang, C. Wang, Y. Liang, S. Yang, L. Wang, S. Wang, Digital twin-driven industrialization development of underwater gliders, IEEe Trans. Industr. Inform. (2023), https://doi.org/10.1109/TII.2023.3233972.
[14] A.K. Dewangan, S.Q. Moinuddin, M. Cheepu, S.K. Sajjan, A. Kumar, Thermal Energy Storage: opportunities, Challenges and Future Scope, in: A. Kumar, V. P. Singh, C.S. Meena, N. Dutt (Eds.), Thermal Energy Systems: Design,

Computational Techniques and Applications, CRC Press, Boca Raton, FL, USA, 2023, pp. 17–28, https://doi.org/10.1201/9781003395768-2. Chapter 2.
[15] T. Sarpkaya, A critical review of the intrinsic nature of vortex-induced vibrations, J. Fluids. Struct. 19 (4) (2004) 389–447.
[16] A. Khalak, C.H.K. Williamson, Motions, forces and mode transitions in vortex-induced vibrations at low mass-damping, J. Fluids. Struct. 13 (7–8) (1999) 813–851.
[17] R. Govardhan, C.H.K. Williamson, Modes of vortex formation and frequency response of a freely vibrating cylinder, J. Fluid. Mech. 420 (2000) 85–130.
[18] Z. Shangyan, O. Abdelkhalik, A Numerical Simulation of a Variable-Shape Buoy Wave Energy Converter, J. Mar. Sci. Eng 9 (6) (2021) 625.
[19] M. Jafari, A. Babajani, P. Hafezisefat, M. Mirhosseini, A. Rezania, L. Rosendahl, Numerical simulation of a novel ocean wave energy converter, Energy Procedia 147 (2018) 474–481, https://doi.org/10.1016/j.egypro.2018.07.050.
[20] S. Huang, M. Huang, Y. Lyu, Seismic performance analysis of a wind turbine with a monopile foundation affected by sea ice based on a simple numerical method, Eng. Appl. Comput. Fluid Mech. 15 (1) (2021) 1113–1133, https://doi.org/10.1080/19942060.2021.1939790.
[21] W. Chen, W. Liu, H. Liang, M. Jiang, Z. Dai, Response of storm surge and M2 tide to typhoon speeds along coastal Zhejiang Province, *Ocean Eng.*, Volume 270, 113646, https://doi.org/10.1016/j.oceaneng.2023.
[22] L. Yin, L. Wang, L. Ge, J. Tian, Z. Yin, M. Liu, W. Zheng, Study on the thermospheric density distribution pattern during geomagnetic activity, Appl. Sci. 13 (9) (2023), https://doi.org/10.3390/app13095564.
[23] L. Yin, L. Wang, T. Li, S. Lu, Z. Yin, X. Liu, W. Zheng, U-Net-STN: a Novel end-to-end lake boundary prediction model, Land. (Basel) 12 (8) (1602) 2023, https://doi.org/10.3390/land12081602.
[24] K. Liao, D. Lu, M. Wang, J. Yang, A low-pass virtual filter for output power smoothing of wind energy conversion systems, IEEE Trans. Ind. Electron. 69 (12) (2023) 12874–12885, https://doi.org/10.1109/TIE.2021.3139177.
[25] X. Lin, Y. Liu, J. Yu, R. Yu, J. Zhang, H. Wen, Stability analysis of Three-phase Grid-Connected inverter under the weak grids with asymmetrical grid impedance by LTP theory in time domain, Int. J. Electr. Power Energy Syst. 142 (2022) 108244, https://doi.org/10.1016/j.ijepes.2022.108244.
[26] A.K. Paul, A. Prasad, A. Kumar, Review on artificial neural network and its application in the field of engineering, *J. Mech. Eng.: PRAKASH*, Vol. 1 (1), 53–61, https://doi.org/10.56697/JMEP.2022.1107.
[27] V. Verma, S. Thangavel, N. Dutt, A. Kumar, R. Weerasinghe, *Highly Efficient Thermal Renewable Energy Systems: Design, Optimization and Applications*, First Edition, CRC Press, Boca Raton, FL USA, 2024, https://doi.org/10.1201/9781003472629.
[28] X. Lin, Y. Wen, R. Yu, J. Yu, H. Wen, Improved weak grids synchronization unit for passivity enhancement of grid-connected inverter, IEEe J. Emerg. Sel. Top. Power. Electron. 10 (6) (2022) 7084–7097, https://doi.org/10.1109/JESTPE.2022.3168655.
[29] J. Jiang, L. Zhang, X. Wen, E. Valipour, S. Nojavan, Risk-based performance of power-to-gas storage technology integrated with energy hub system regarding downside risk constrained approach, Int. J. Hydrogen. Energy 47 (93) (2022) 39429–39442, https://doi.org/10.1016/j.ijhydene.2022.09.115.
[30] J.Zhang L.Lin, X. Gao, J. Shi, C. Chen, N. Huang, Power fingerprint identification based on the improved V-trajectory with color encoding and transferred CBAM-ResNet, PLoS. One 18 (2) (2023) e0281482, https://doi.org/10.1371/journal.pone.0281482.
[31] K. Vikestad, J.K. Vandiver, C.M. Larsen, Added mass and oscillation frequency for a circular cylinder subjected to vortex-induced vibrations and external disturbance, J. Fluids. Struct. 14 (7) (2000) 1071–1088.
[32] W. Wei, M.M. Bernitsas, K. Maki, RANS simulation versus experiments of flow induced motion of circular cylinder with passive turbulence control at 35,000< Re< 130,000, J. Offshore Mech. Arct. Eng. 136 (4) (2014) 041802.
[33] S.Arora Priyanka, F.M. Oudina, S. Sahani, Super convergence analysis of fully discrete Hermite splines to simulate wave behaviour of Kuramoto–Sivashinsky equation, Wave Motion. 121 (2023) 103187, https://doi.org/10.1016/j.wavemoti.2023.103187.
[34] Q. Yang, W. Piguang, F. Shixiao, Z. Mi, Numerical study on vortex-induced vibrations of a flexible cylinder subjected to multi-directional flows, Phys. Fluids 35 (3) (2023), https://doi.org/10.1063/5.0138063, 037104-037104.
[35] A. Kumar, Y. Gori, N. Dutt, Y.K. Singla, A. Maurya, *Advanced Computational Methods in Mechanical and Materials Engineering*, First Edition, CRC Press, Boca Raton, FL USA, 2021, https://doi.org/10.1201/9781003202233.
[36] A. Kumar, V.P. Singh, C.S. Meena, N. Dutt, *Thermal Energy Systems: Design, Computational Techniques and Applications*, First Edition, CRC Press, Boca Raton, FL USA, 2023, https://doi.org/10.1201/9781003395768.
[37] A.F. Jozaei, A. Alizadeh, A. Ghafouri, Modelling of the Dynamics of an immersed body in a microchannel with stenosis using the immersed boundary method, J. Appl. Comput. Mech. 50 (2) (2019) 228–238, https://doi.org/10.22059/jcamech.2018.243247.193.
[38] M.K. Awasthi, A.K. Shukla, A. Kumar, D. Yadav, N. Dutt, Viscous correction to the potential flow analysis of Rayleigh–Taylor instability in a Rivlin–Ericksen viscoelastic fluid layer with heat and mass transfer, Heat Transf. (2024) 1–17, page, https://onlinelibrary.wiley.com/doi/10.1002/htj.23076.
[39] M. Maleki, S.H. Dibajian, A.R. Bastami, M. Rajabi, Influence of booster's geometry and circuit's resistor on performance of the auxetic energy harvester - experimentally validated analysis, J. Appl. Comput. Mech. 54 (4) (2023) 467–481.
[40] A.P. Pandey, A. Sawla, S. Kr. Gupta, P. Baredar, Vivec (Vortex induced vibration energy converter): a New and renewable approach to harness the hydro-kinetic energy of geophysical fluid flow, Int. J. Adv. Sci. Res. Sci. Eng. 5 (3) (2020).
[41] Shitong Fang, Houfan Du, Tao Yan, Keyu Chen, Zhiyuan Li, Xiaoqing Ma, Zhihui Lai, Shengxi Zhou, Theoretical and experimental investigation on the advantages of auxetic nonlinear vortex-induced vibration energy harvesting, Appl. Energy 356 (2024).
[42] P. Xu, S. Jia, D. Li, O. el Moctar, C. Jiang, Optimization Study of Marine Energy Harvesting from Vortex-Induced Vibration Using a Response-Surface Method, J. Mar. Sci. Eng. 11 (3) (2023) 668, https://doi.org/10.3390/jmse11030668.
[43] M.K. Awasthi, N. Dutt, A. Kumar, S. Kumar, Electrohydrodynamic capillary instability of Rivlin–Ericksen viscoelastic fluid film with mass and heat transfer, Heat Transf. 53 (1) (2024) 115–133, https://doi.org/10.1002/htj.22944.
[44] P.N. Reddy, V. Verma, A. Kumar, M. Awasthi, Simulation and thermal performance optimization of flow in a channel with multiple baffles, J. Heat Mass Transf. Res. 10 (2) (2023) 257–268, https://doi.org/10.22075/JHMTR.2023.31108.1458.
[45] M. Ahmadizadeh, M. Heidari, S. Thangavel, E.A. Naamani, M. Khashehchi, V. Verma, A. Kumar, Technological Advancements in Sustainable and Renewable Solar Energy Systems, CRC Press, Boca Raton, FL, USA, 2024, pp. 23–39, https://doi.org/10.1201/9781003472629-2, 2024; Chapter 02.
[46] A. Saxena, A.N Prajapati, G. Pant, C.S. Meena, A. Kumar, V.P. Singh, Water Consumption Optimization of Hybrid Heat Pump Water Heating System. Lecture Notes in Mechanical Engineering, Springer, Singapore, 2023, https://doi.org/10.1007/978-981-99-1894-2_61.
[47] A. Bansal, H.K. Bhardwaj, V.K. Sharma, A. Kumar, Static and dynamic behavior analysis of Al-6063 alloy using modified Hopkinson bar. Additive Manufacturing in Industry 4.0: Methods, Techniques, Modeling and Nano Aspects, CRC Press, Boca Raton, FL, USA, 2022, pp. 107–124, https://doi.org/10.1201/9781003360001-6. Chapter 6.
[48] S. Rana, A. Kumar, Y. Gori, P. Patil, Design and analysis of thermal contact conductance, J. Crit. Rev. 6 (5) (2019) 363–370, p.n.
[49] S. Fardin, Md.J. Moresalein, Md.S.A. Aziz, S. Saha, Md.N. Hasan, Role of periodic oscillating flow modulators on mixed convection in a long horizontal channel, Int. J. Thermofluids. 24 (2024) 100817, https://doi.org/10.1016/j.ijft.2024.100817.
[50] Balram Mandal, Roshani Kumari Gupta, Abhinav Adhikari, Mit Manojbhai Sheth, Rameshkumar Bhoraniya, Atal Bihari Harichandan, Computational study of vortex shedding and its effects on asymmetrical airfoil with gurney flap, Int. J. Thermofluids. 24 (2024) 100796, https://doi.org/10.1016/j.ijft.2024.100796.
[51] S. Bilal, Muhammad Yasir, Muhammad Bilal Riaz, Thermal characteristics of Falkner-Skan flow of time-dependent Maxwell material with varying viscosity and thermal conductivity, Int. J. Thermofluids. 24 (2024) 100833, https://doi.org/10.1016/j.ijft.2024.100833.
[52] Jithender Reddy Gurejala, Manideep Pampera, Raja shekhar pemmaraju, srinivasa raju rallabandi, impact of viscous dissipation on MHD flow of Maxwell nanofluid across a linear stretching sheet, Int. J. Thermofluids. 24 (2024) 100832, https://doi.org/10.1016/j.ijft.2024.100832.
[53] Sadib Fardin, Md.Jawarul Moresalein, Md.Samin Ashiq Aziz, Sumon Saha, Mohammad Nasim Hasan, Role of periodic oscillating flow modulators on mixed convection in a long horizontal channel, Int. J. Thermofluids. 24 (2024) 100817, https://doi.org/10.1016/j.ijft.2024.100817.